Bio-Inspired Multiproperty Materials: Strong, Self-Healing, and Transparent Artificial Wood Nanostructures

Rémi Merindol,[†,‡] Seydina Diabang,[†] Olivier Felix,[*,†] Thierry Roland,[†,⊥] Christian Gauthier,[†,§] and Gero Decher[*,†,‡,∥]

[†]CNRS - Institut Charles Sadron (UPR22), 23 rue du Loess, F-67034 Strasbourg, France, [‡]Faculté de Chimie, Université de Strasbourg, 1 rue Blaise Pascal, F-67008 Strasbourg, France, [§]UFR de Physique, Université de Strasbourg, 4 rue Blaise Pascal, F-67081 Strasbourg, France, [⊥]INSA de Strasbourg, 24 Bd de la Victoire, F-67084 Strasbourg, France, and [∥]International Center for Frontier Research in Chemistry, 8 allée Gaspard Monge, F-67083 Strasbourg, France

ABSTRACT Nanocomposite films possessing multiple interesting properties (mechanical strength, optical transparency, self-healing, and partial biodegradability) are discussed. We used Layer-by-Layer assembly to prepare micron thick wood-inspired films from anionic nanofibrillated cellulose and cationic poly(vinyl amine). The film growth was carried out at different pH values to obtain films of different chemical composition, whereby, and as expected, higher pH values led to a higher polycation content and also to 6 times higher film growth increments (from 9 to 55 nm per layer pair). In the pH range from 8 to 11, micron thick and optically transparent LbL films are obtained by automated dipping when dried regularly in a stream of air. Films with a size of 10 cm^2 or more can be peeled from flat surfaces; they show tensile strengths up to about 250 MPa and Young's moduli up to about 18 GPa as controlled by the polycation/polyanion ratio of the film. Experiments at different humidities revealed the plasticizing effect of water in the films and allowed reversible switching of their mechanical properties. Whereas dry films are strong and brittle (Young's modulus: 16 GPa, strain at break: 1.7%), wet films are soft and ductile (Young's modulus: 0.1 GPa, strain at break: 49%). Wet film surfaces even amalgamate upon contact to yield mechanically stable junctions. We attribute the switchability of the mechanical properties and the propensity for self-repair to changes in the polycation mobility that are brought about by the plastifying effect of water.

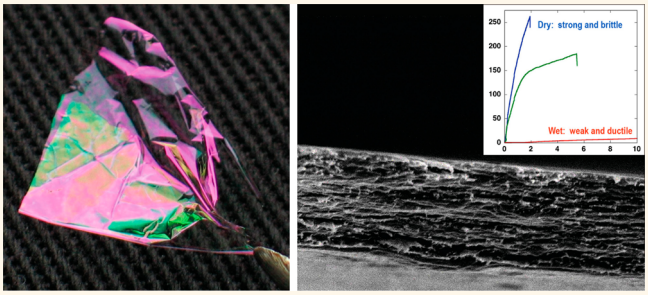

KEYWORDS: Layer-by-Layer assembly · nanofibrillated cellulose · artificial wood · bio-inspired nanostructures · multiproperty materials · mechanical properties · self-healing · transparent coatings

The great strength of Layer-by-Layer (LbL)-assembled films[1] is based on the ease by which multimaterial nanocomposites can be prepared and structurally controlled. A classic concept for improving the mechanical properties of a material is to combine so-called reinforcing agents with a polymer matrix,[2,3] which is often realized in the form of a dispersion. However, such dispersions often have a tendency to demix, which strongly decreases their optical transparency and which also degrades the "reinforcing effect" that depends on optimum distances of individual reinforcing objects in the matrix material. Kotov *et al.* have shown that two-material nanocomposites with record mechanical strengths can be obtained by LbL assembly of polymers and clay platelets[4,5] or carbon nanotubes.[6] The advantage of LbL assembly for the preparation of nanocomposites is that the structure of the composite films is based on the deposition sequence (which determines the layer sequence) and the deposition conditions (which control, for example, the adsorbed amounts per layer). The fact that LbL films require the different components in adjacent layers to interact with each other attractively helps to prevent or at least diminish phase separation and demixing. Consequently, some LbL films maintain their structure and properties over several years. On the other hand, the charges in weak polyelectrolytes can be gradually switched on or off by changing the pH of the environment. By doing this, the charge density along the polymer backbone can be

* Address correspondence to decher@unistra.fr, olivier.felix@ics-cnrs.unistra.fr.

Received for review August 6, 2014 and accepted December 18, 2014.

Published online January 15, 2015
10.1021/nn504334u

varied, and thus the strength of the interaction with the neighboring counter-polyion can be fine-tuned.[7] We have therefore chosen a reinforcing agent carrying weak anionic groups (carboxyl groups) (anionic nanofibrillated cellulose, CNF) in combination with a weak polycation (poly(vinyl amine), PVAm) (Chart 1) as matrix polymer which is used in the paper industry and which is known to improve the dry or wet strength of paper.[8]

The fact that wood is a biodegradable material with excellent mechanical properties controlled by its composition[9] and structure[10] gave rise to the hope that the LbL assembly of this polyanion/polycation pair would lead to a fiber-reinforced nanocomposite whose mechanical properties could be fine-tuned through a simple variation of the pH during the preparation of the composite material while maintaining a good control of its nanostructure through the LbL assembly process. In collaboration with Wågberg, we had already shown that the combination of anionic CNFs with poly(ethylene imine) leads to LbL films with good structural control as demonstrated by the observation of optical interference colors that are stable over prolonged periods of time.[11] Such "structural colors" are only observed with objects that are optically homogeneous with respect to their thickness and their refractive index and are therefore also a qualitative indicator for structural homogeneity.

The preparation of artificial wood nanostructures that we introduce here is based on the Layer-by-Layer deposition of CNF and PVAm at different pH on silicon wafers by dipping. As expected, the growth of such films turned out to be sensitive to the pH of PVAm solution that controls the charge density of PVAm, its conformation, and its content in the multilayers. Higher pH values led to a transition from nearly linear to superlinear growth, a higher polycation content, and up to 6 times higher growth increments (from 9 to 55 nm). Optically transparent thick freestanding films prepared in the pH range from 8 to 11 were peeled from modified silicon wafers, and their mechanical properties were studied as a function of the pH and the relative humidity. Higher pH led to higher Young's moduli and lower strains at break, while the tensile strengths stay in the range of the best CNF-based materials (200−250 MPa). As humidity increases, Young's modulus and strain of the film decrease while strain at break increases. The switchability of the mechanical properties and the propensity for self-healing could be attributed to changes in the polycation mobility (interaction strength between the building blocks) that are brought about the plastifying effect of water. An enhanced polyelectrolyte mobility in LbL films was already reported to enable self-healing in water.[12] Strong LbL-assembled films with structural control and self-repair abilities are a new milestone toward high technology applications in the growing field of nanocellulose-based materials.[13,14]

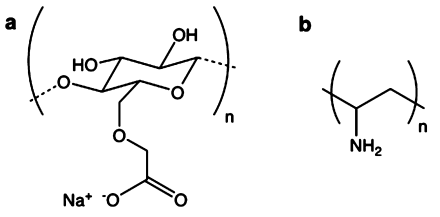

Chart 1. Chemical structures of anionic nanofibrillated cellulose (a) and poly(vinyl amine) (b).

RESULTS AND DISCUSSION

Control of PVAm Content in the Films by the pH. The pH of the PVAm solution was varied from 8 to 11 during construction of the LbL films on silicon wafers, while the pH values for the CNF suspension and for the rinsing solution were kept constant at pH = 6.0 ± 0.5 (Figure 1).

As the charge density of the PVAm is reduced with higher pH, PVAm is increasingly incorporated into the LbL film; a 6 layer pair film built at pH = 8 was 35 ± 1 nm

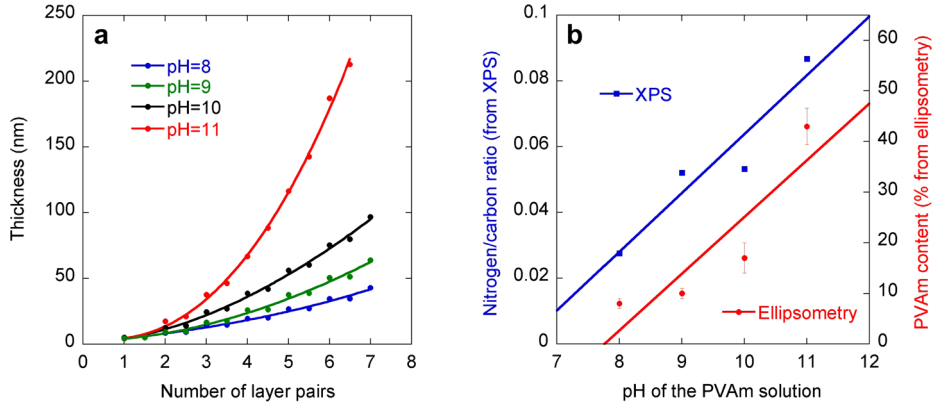

Figure 1. (a) Buildup of LbL films as a function of the pH of the PVAm solution followed by ellipsometry on activated silicon wafers. Error bars are smaller than the size of the data points. (b) Content of PVAm in the films built at different pH values. (Blue) Ratio of the integral under the N 1s and C 1s peaks in the XPS spectra of micron thick films with CNF as last layer. (Red) Percentage of the ellipsometric thickness increase for the PVAm layer. Solid lines have no physical meaning and are only a guide for the eye.

thick while a 6 layer pair film built at pH = 11 was 187 ± 10 nm. Simultaneously, the growth regime of the film changes from nearly linear to superlinear. This phenomenon, reported for CNF in combination with poly(ethylene imine)[15] and other polyelectrolyte couples,[7,16,17] is related to the decrease of the charge of the PVAm (pK_a around 10) and very likely to the conformational change of the PVAm chains from extended to coil with increasing pH, while the CNFs bearing carboxylic groups (pK_a around 4.5) do not see their degree of ionization modified in the studied pH range.[18] As the charge on the PVAm chains decreases, the amount of PVAm adsorbing on reference cellulose surfaces increases.[19] An increase of the thickness increment during multilayer buildup was also reported when salt is added to the polymer solution[11,15] or when the degree of ionization of the polymer decreases.[20]

For the case of a solution, it is accepted that the reduction of electrostatic repulsion along the polyelectrolyte backbone, which is brought about by either decreasing the charge density along the polymer chain or increasing the ionic strength of the solution, leads to a change of the polyelectrolyte conformation from extended to coil-like. While this argument may not be fully valid for estimating the polyelectrolyte conformation in a polyelectrolyte complex and therefore also not in a polyelectrolyte multilayer, it has frequently been observed that a reduction in charge density or an increase of the ionic strength leads to thicker LbL films in which the polyelectrolyte conformation is likely a flattened coil. When the charge density decreases, the mobility of the PVAm in the film increases, probably due to reduced electrostatic interactions between the CNFs and the PVAm, which also seems to promote superlinear growth which was already observed at high pH.[7] Note that we only adjusted the pH in the PVAm solution, and in all experiments, we rinsed with pure water (pH = 6.0) to prevent salt crystallization during drying. The solutions of CNF were also kept at a pH of 6 to prevent colloidal destabilization. Under these experimental conditions, we observed a clear effect of the pH on the construction of the films; the superlinear growth may have been amplified by the alternation of high and low pH.[21]

Ellipsometry also reveals that the volume fraction of PVAm in the film (thickness increment of PVAm divided by the thickness increment of the layer pair) increases with the pH (Figure 1b). This observation is coherent with previously reported results on other films.[22] To corroborate our ellipsometric data, we recorded the X-ray photoelectron spectroscopy (XPS) spectra of similar micron thick films prepared by dipping with CNF as the last layer. By increasing the pH of the PVAm solution, the area under the peak of the 1s orbital of nitrogen increases as compared to the area under the peak of the 1s orbital of carbon, revealing that the content of nitrogen on the surface is multiplied by a factor of about 3 as the pH is increased from 8 to 11. Morphology of $(PVAm/CNF)_8$ films built at pH = 8 and 11 by dipping is shown in Supporting Information (Figure S1). Note that the effect of this controlled variation of the film composition with respect to PVAm (energy-dissipating matrix) and CNF (nanoreinforcing component) on mechanical properties of such films will be discussed in this article.

Construction and Characterization of Thick LbL Films. Our equipment for mechanical tests (tensile strength) was designed for a force range of 0.05 to 2.5 N and requires, therefore, to work with films with a thickness in the micron range. The preparation of homogeneous films in this thickness range required several optimizations, especially at the different pH values. Another challenge is the preparation of thick freestanding LbL films. The use of hydrofluoric acid to dissolve the glass substrate[4] is not possible here as it would damage cellulose fibers in the film. Another way to detach a thin film from its support consists of surface modification of a silicon wafer with fluorinated or alkyl chains, allowing film construction with similar growth as compared to classic activated silicon wafers.[23] In our case, however, the construction of a thick film on such modified substrates led to the formation of crack patterns on the surface of the film. At pH = 8, the first cracks appeared at a film thickness of about 600 nm, making the mechanical tests impossible. The apparition of cracks is probably due to the shrinking of the film upon drying in combination with poor adhesion on the hydrophobized silicon substrate. We noticed that the appearance of cracks in the film was pH-sensitive; increasing the pH lowered significantly the number of cracks. Apparently, as the amount of polymer in the film increases, the stress generated by drying decreases; this probably also explains why previously reported films containing about 20% of poly(ethylene imine) did not crack.[23]

The construction of multilayers directly on a hydrophobic silicon wafer has already been reported for LbL films composed of clays and poly(vinyl alcohol).[24] In this study, we used one layer pair of this clay-based system to enhance the adhesion of our film on the hydrophobic substrate. While this adhesion-promoting layer had only negligible influence on the film growth, it made it possible to build micron thick films without cracks. We believe that this combination of hydrophobic substrate and adhesion layer could be widely used for the general preparation of freestanding LbL films and likely for other types of films, as well. Hydrophobic substrates covered with clay present a surface very similar to the one of the activated silicon wafer traditionally used in LbL deposition. Films deposited on top of theses substrates can then be easily removed using tape or tweezers due to the weak adhesion of the film on the substrate.

The scanning electron microscopy (SEM) image and the profile obtained by atomic force microscopy (AFM)

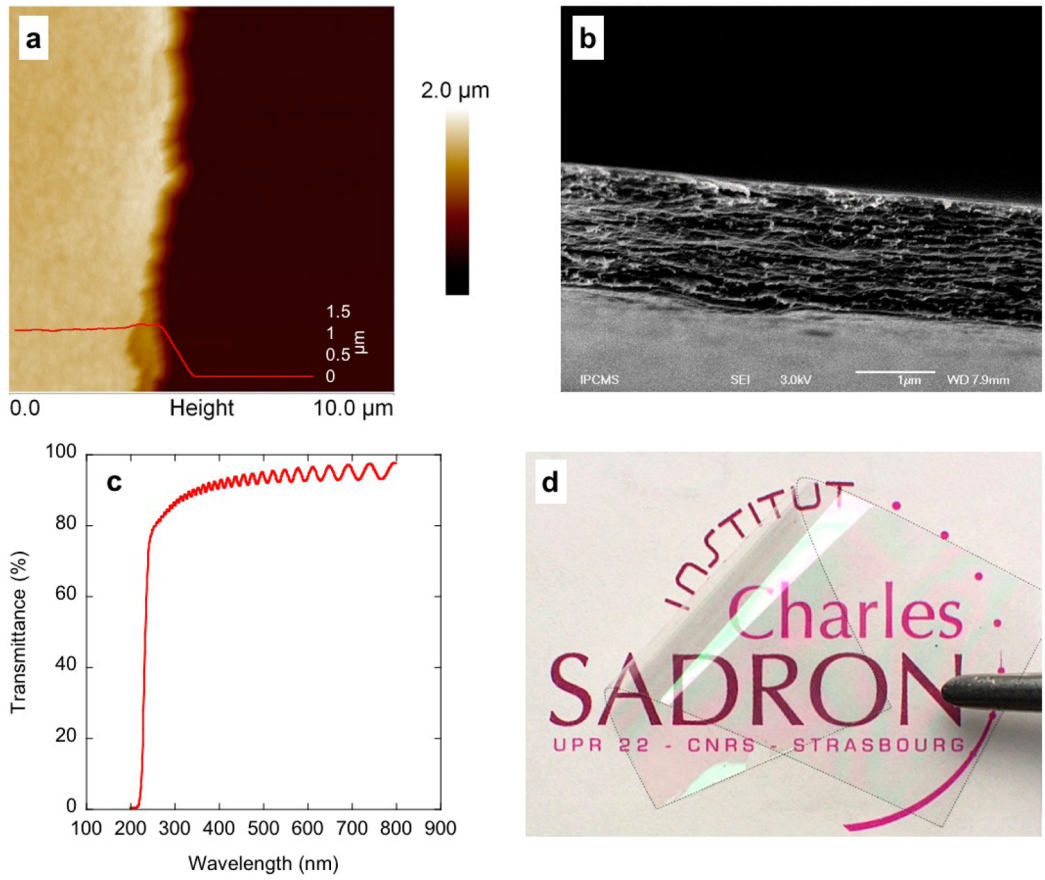

Figure 2. (a) AFM image and profile (insight in red) of the edge of a $(PVAm/CNF)_{70}$ film built from a PVAm solution at pH = 9 resting on a silicon wafer (brown background on the right). The profile was taken roughly on the middle of the image. A film thickness of 1.1 μm is observed by AFM and is in agreement with that measured by spectroscopic ellipsometry (1.1 $\pm$ 0.1 μm). (b) Cross-section SEM image of a $(PVAm/CNF)_{30}$ film built from a PVAm solution at pH = 11. A film thickness of 1.6 μm is observed by SEM and corresponds to that measured by spectroscopic ellipsometry (1.6 $\pm$ 0.1 μm). (c) UV−vis spectrum of a freestanding $(PVAm/CNF)_{75}$ film built from a PVAm solution at pH = 10. The film thickness obtained by spectroscopic ellipsometry is 3.4 $\pm$ 0.1 μm. (d) Optical photograph of a $(PVAm/CNF)_{60}$ film built from a PVAm solution at pH = 10.5. The film thickness measured by spectroscopic ellipsometry is 3.8 $\pm$ 0.1 μm. The edges of the film are marked with a dotted line to facilitate the observation of the film borders.

(Figure 2a,b) are representative examples of the different freestanding LbL films obtained. The in-plane orientation of cellulose nanofibrils in the film can be clearly seen by SEM using a secondary electron detector. All methods used confirm that films prepared are uniformly thick, homogeneous, and rather smooth. In order to obtain smooth edges for microscopy, the film were notched and carefully torn. The use of a scalpel gave, in some cases, rough edges that prevented accurate thickness measurements. The AFM profile shows a bump near the edge, which is caused by accumulation of material during cutting. One can also observe on the edge at the bottom of the image an intermediate step on the edge of the film, which is typical of layered materials. Thicknesses determined by scanning electron microscopy and by spectroscopic ellipsometry are very close, underlining the accuracy of the model used for spectroscopic ellipsometry (constant refractive index equal to 1.55). Please note that the cross-section SEM images of PVAm/CNF films assembled at pH 8 (low PVAm content) and pH 11 (high PVAm content) show only minor structural differences due to the limited resolution of the technique.

The UV−visible transmittance of a $(PVAm/CNF)_{75}$ freestanding film was recorded in the spectral range from 200 and 800 nm (Figure 2c). The film shows a high transparency in the visible spectrum with over 85% transmittance, while it strongly absorbs below 250 nm. Contrary to films prepared by vacuum filtration,[25] the film does not require any additional treatment to be transparent. The UV−visible spectrum also displays typical Fabry-Perrot fringes, confirming the excellent homogeneity of the film thickness and refractive index.[26] The image (Figure 2d) confirms the high transparency of the film. One can also distinguish shades of green and pink on the picture; these colors come from interferences and are typically observed for thin films with uniform thickness and low surface roughness. These films can be easily manipulated and folded without breaking.

Mechanical Characterization of the Freestanding Films. The mechanical properties of the $(PVAm/CNF)_n$ films built

TABLE 1. Mechanical Characteristics of Micron Thick Films Built from PVAm Solutions at pH Ranging from 8 to 11

pH	number of layer pairs	thickness (μm)	Young's modulus (GPa)	stress at break (MPa)	strain at break (%)
8	150	1.35 (±0.01)	12.1 (±1.8)	206 (±66)	4.7 (±3.1)
9	70	1.12 (±0.05)	11.9 (±1.1)	209 (±19)	8.9 (±2.6)
10	30	1.02 (±0.03)	17.7 (±0.6)	197 (±27)	2.5 (±1.8)
11	30	1.65 (±0.07)	16.5 (±1.5)	141 (±43)	0.9 (±0.4)

from different PVAm solutions were systematically studied by varying the ratio of polymer to nanoreinforcing component. In order to get comparable values for the different films, the number of layer pairs was adjusted to have a similar total thickness for all the films (from 1.0 to 1.6 μm).

The mechanical characteristics obtained for these materials (Table 1) are in the range of the best CNF-based material[25,27] and are approaching the strongest LBL-based materials (400 MPa).[4] We found that the Young's modulus of the film was sensitive to the pH of PVAm solution during film construction; at pH = 8 and 9, the modulus was around 12 GPa, while at pH = 10 and 11, we found a modulus around 17 GPa.

We attribute this increase to a better reinforcing efficiency of the embedded CNFs as the content of PVAm increases (Figure 2). Similarly, films built at pH = 8 and 9 had a lower yield strength than the film built at pH = 10, and the film built at pH = 11 always broke before yielding (Figure 3). There is probably an optimum PVAm/CNF ratio for obtaining the best mechanical reinforcement. At very low PVAm content, there are only few polymer chains bridging neighboring fibrils, and this results in a low Young's modulus and a low yield point. As the amount of PVAm in the film increases, more bridges are created between adjacent cellulose nanofibrils and the reinforcing efficiency of each fibril increases, which results in a slight overall increase of the Young's modulus despite the lower CNF content. The weaker interaction between the fibrils at low pH may allow for the fibers to rearrange before fracture, which could result in higher toughness. It is also possible that these changes are partially caused by a modification of the conformation of the PVAm chains in the film, with a more coil-like shape at high pH and a more extended conformation at low pH. In this case, a more coiled polymer conformation could result in a better stress repartition along the CNF fibers, which could also explain the higher modulus of the film assembled at high pH.

When the content in PVAm increases, there are less weak fiber/fiber interactions and more strong fiber/PVAm interactions; therefore, the Young's modulus and the yield strength increase. At pH = 10, an optimum composition seems to be reached with a high Young's modulus, a high strength, and a large growth increment. However, some samples (built at pH 8 or 9) reached a strength above 230 MPa, these very high values are attributed to the high toughness of these

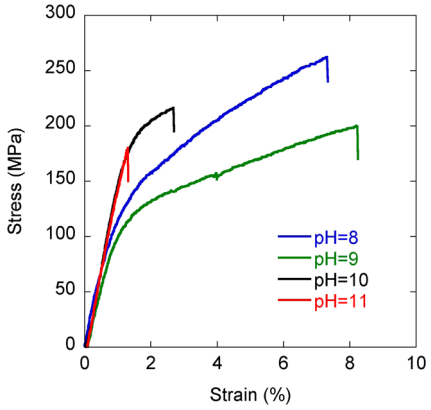

Figure 3. Typical stress–strain curves obtained for micron thick $(PVAm/CNF)_n$ films built from PVAm solutions at pH ranging from 8 to 11.

films arising from their high CNF content as compared to films built at higher pH. The relatively large error bars obtained for these measurements are due to the difficulty obtaining perfectly smooth edges during sample preparation that leads to premature breaking of the film. In any case, the general profile of the tensile curves obtained for films built at one given pH is characteristic. Similar mechanical tests on multilayers containing cationic nanofibrillated cellulose and poly(acrylic acid) deposited at pH = 3 displayed similar mechanical properties with strength reaching 250 MPa.

The strength and modulus of the different films are higher than what was found by Wågberg *et al.*[11] for freestanding CNF-based films. They attributed the low strength of their films to the absence of humidity. We addressed this problem by measuring the mechanical properties of the films in different humidity conditions.

Using Water as a Plasticizing Agent. Water is known to have a strong plasticizing effect on polyelectrolyte complexes.[28] Therefore, we studied the effect of relative humidity (RH) on the mechanical properties of a film built at pH = 10 (Figure 4 and Table 2). In order to measure the mechanical properties at wet conditions (low strength), a thicker film was needed for these experiments.

The general trend of humidity can be clearly seen on the stress–strain curves (Figure 4a). As humidity increases, strength and Young's modulus of the film decrease while the strain at break increases. This effect can be mostly attributed to the nature of the interactions in the material (Figure 4b).

At low RH, there is very little water in the film; the electrostatic and hydrogen bonding interactions

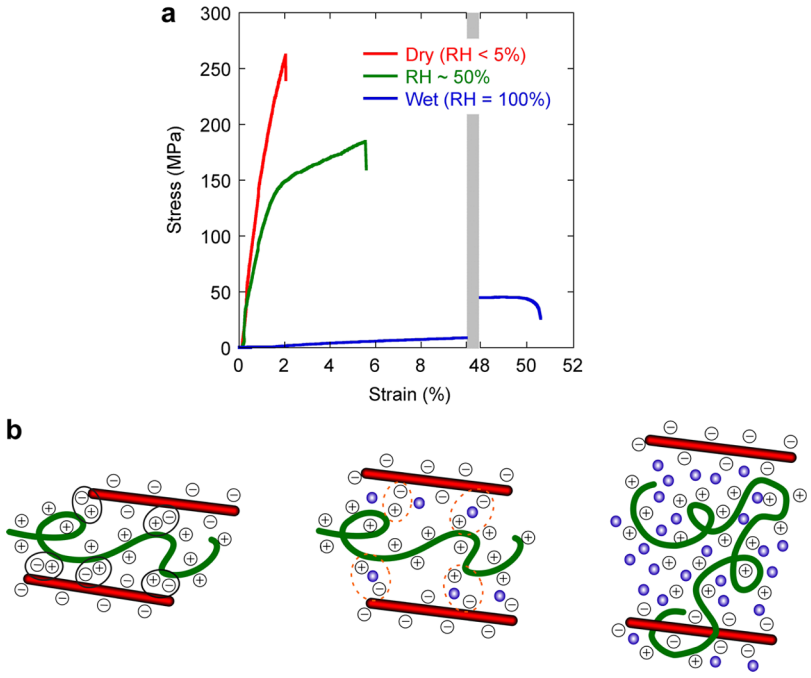

Figure 4. (a) Typical stress−strain curves obtained for $(PVAm/CNF)_n$ thick films (3.4 ± 0.1 μm) built from PVAm solution at pH = 10 in various humidity conditions. Note that the *x*-axis was interrupted between 10 and 48% for clarity. (b) Simplified molecular sketch of the effect of hydration on the interactions between CNF and PVAm. The green lines represent PVAm; the red sticks correspond to CNF, and the blue dots represent the water molecules in the film; + and − symbols represent, respectively, pending ammonium and carboxylates groups (counterions have been omitted for clarity).

TABLE 2. Mechanical Characteristics of Thick $(PVAm/CNF)_n$ Films (3.4 ± 0.1 μm) Built from PVAm Solution at pH = 10 in Various Humidity Conditions

humidity	Young's modulus (GPa)	stress at break (MPa)	strain at break (%)
<5%	16 (±3)	237(±31)	1.7 (±0.4)
~50%	12 (±2)	174 (±20)	3.3 (±2.2)
wet (100%)	0.12 (±0.01)	46 (±11)	49 (±8)

among the CNF fibers,[29] among the polymer chains and between the fibers and the PVAm, are strong, and the PVAm is rigid. This leads to a very strong composite, reaching the strengths of the best CNF-based materials with low maximal strain and no plastic deformation. Compared to previously reported CNF-containing LbL films,[23] these films have higher Young's modulus and strength. We attributed this to the strong bonding of PVAm to the cellulose.[30] Long linear polymers are also known to reach higher strength than dendrimers as they reach higher degrees of entanglements for similar molecular weight.[31] The humidity conditions at which we performed the mechanical tests are also slightly higher (~3%) than those used by Wågberg and coworkers (~0%), but a lower humidity appears to increase the maximal strength.

At ambient conditions (RH ~ 50%), the film absorbs some water. As a consequence, the electrostatic interactions and the hydrogen bonds between CNF and PVAm (and among CNF fibers) decrease and the poly(vinyl amine) is partially plastified, but interestingly, the Young's modulus is not much affected (Table 2). This is in agreement with theories for macrocomposites with high aspect ratio fibers.[31] It seems that, because the ratio of reinforcing CNFs to PVAm is constant, the Young's modulus also stays constant despite an increased PVAm mobility due to the plastifying action of the water. However, the reduced interaction between the PVAm and the CNFs is the reason why the maximum strength and also the yield strength of our composite films decrease.

Interestingly, recent experiments on LbL films composed of poly(ethylene imine) and anionic nanofibrillated cellulose revealed a different behavior.[32] This difference could be explained by the polycations used, poly(vinyl amine) in our case, which is known to enhance the wet strength to paper,[30] and poly(ethylene imine) in ref 32, which may be more sensitive to humidity. Another explanation for the different results may be related to the techniques used for determining the mechanical properties; buckling mechanics and tensile strength testing may lead to different interpretations when applied to lamellar composites.[33]

At ambient humidity conditions, the films yield around 150 MPa and reach strains up to 6%. The plastic deformation can be explained according to shear-lag theories[34] with sliding at the interface between the fibers and the PVAm or plastic deformation of the PVAm. Both phenomena would be promoted by the increase of humidity as water can either plastify PVAm

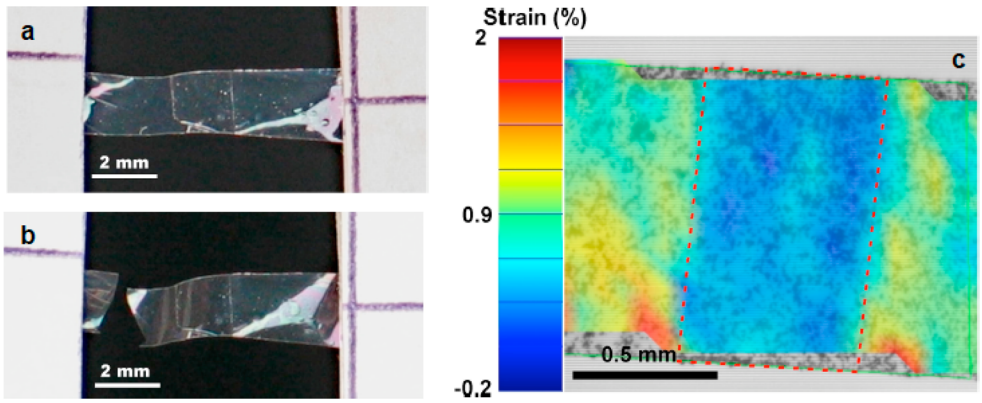

Figure 5. Image of a self-repaired film before (a) and after (b) pulling on it. (c) Visualization of the deformation of a repaired film by image correlation. The image extracted from the video (gray scale) displays the film with black patterns coming from printer toner deposited on it. The colors added by the correlation software, show low deformation regions in blue and high deformation regions in orange. The overlap region is outlined in dashed red.

or screen the electrostatic interactions between the fiber and the polymer matrix.

In wet conditions (RH = 100%), the film swells and the electrostatic interactions and hydrogen bonds between CNF and PVAm are greatly decreased and the PVAm is highly hydrated, allowing for rearrangements and diffusion in the film. Consequently, the Young's modulus decreases to 120 MPa, and the maximal stress decreases to a quarter of its room humidity value. On the other hand, the maximal strain increases to 50%. The elastic modulus and maximal strain are calculated using the film thickness measured in the dry state; this makes the comparison with other cellulose hydrogels difficult.[35,36] Interestingly, heating the dry film for 12 h at 120 °C before the mechanical test doubled the strength and Young's modulus of the wet film but did not impact significantly the properties at other humidity conditions. The wet strength relies mostly on covalent bonds (such as amide bonds created during thermal treatment), while in the dry state, electrostatic interactions and hydrogen bonds are sufficient to reach high strength.

One notices a lower strength and Young's modulus for this 3.4 μm thick film than for the 1.0 μm thick film built at pH = 10 (Tables 1 and 2). It appears that there was a decrease of the pH of the PVAm solution during deposition. After 30 layer pairs, the pH of the PVAm solution was 9.8, while after 75 layer pairs, it was 9.3. This explains why the mechanical properties of the thicker film are located between the properties of the film built at pH = 10 and at pH = 9. Based on this observation, the conclusions on the changes of mechanical properties with humidity remain valid.

During our investigations, we observed that the films had a tendency to stick to themselves after immersion in water. Since cases of self-repairing LbL materials showing superlinear growth have already been reported in the literature,[12] we carried out a simple self-healing experiment in which the surfaces close to the edges of two wet films were superposed, and this led to the formation of a stable freestanding film (Figure 5a). When carrying out tensile tests on such repaired films, surprisingly, all the samples broke outside the repaired region (Figure 5b). The stress at break obtained for repaired films was 157 $\pm$ 33 MPa, which is comparable to the 174 $\pm$ 20 MPa obtained for native films. On the deformation mapping obtained by digital image correlation (Figure 5c), it appears that the parts of the film adhering together are deforming much less than the rest of the film. The lower deformation in this region reveals a proper healing; the film behaves as if it was a continuous film with a region twice as thick in the middle. We do not observe regions of high and low deformation that would appear if the films were sliding or partially delaminating. The red parts at the bottom of the images come from artifacts in the calculation of deformation at the limits of the area of interest known as edge effects. These self-repairing tests are not a quantitative representation of the self-repairing ability of these materials, but an edge to edge contact was impossible for such thin films and the cellulose nanofibrils prevent lateral diffusion for scratch healing.

The repairing properties observed in wet conditions are enabled by the mobility of the polymer chains in the multilayer in the presence of water. Composite hydrogels showing somewhat similar behavior have been described.[37,38] Films built with poly(acrylic acid) and cationic nanofibrillated cellulose showed similar self-healing behavior when the pH of the poly(acrylic acid) solution was adjusted to 2−3.

SUMMARY AND CONCLUSIONS

This study demonstrates that LbL assembly is capable of producing thick transparent artificial wood nanostructures composed of CNF and PVAm with tunable mechanical performances and a propensity for self-healing. The mechanical properties of such nanocomposites films were tuned through the pH of the PVAm solution during film buildup and the relative humidity of the surrounding environment during

mechanical tests. Chemical composition, growth regime, and thickness of the CNF-based LbL films were controlled by the pH of the PVAm solution. Higher pH values led to higher PVAm content and to 6 times higher film growth increments (from 9 nm at pH = 8 to 55 nm at pH = 11). These films showed tensile strengths up to 250 MPa and Young's moduli up to 18 GPa as controlled by the polycation/polyanion ratio of the film.

External stimuli (changes in humidity) were used to switch the mechanical performance of films prepared at pH 10. While dry films are strong and brittle (tensile strength around 240 MPa, Young's modulus of 16 GPa, and strain at break of 1.7%), wet films are soft and ductile (tensile strength around 50 MPa, Young's modulus 0.1 GPa, and strain at break of 49%). These reversible mechanical property changes are attributed to the plasticizing effect of water controlling the polycation mobility in the films. The latter even leads to the self-healing of wet films upon contact; amalgamated junctions between the two film surfaces show remarkable mechanical stability.

METHODS

Materials. Anionic nanofibrillated cellulose (CNF bearing carboxymethyl functional groups, 515 μequiv g^{-1}, degree of substitution of 0.087) was obtained from Innventia AB (Stockholm, Sweden) as a pulp containing 2.5% of fibers in water. The pulp was mechanically dispersed in Milli-Q water (Milli-Q Gradient system, Millipore, Molsheim, France) to obtain a suspension at 2 g/L and sonicated with tip sonicator (Vibra cell 75042 from Bioblock Scientific, Illkirch, France) for 1 h at 20% amplitude. The resulting suspension was centrifugated for 3 h at 5000 rpm (centrifuge 4K10 with Rotor Nr 12254 from Sigma, Lyon, France), and the resulting supernatant was used as deposition solution after filtration on cotton wool. Typical concentration was in the range of 0.9 g/L as determined from dry mass measurement.

Poly(vinyl amine) (trade name LUPAMIN 9095, PVAm, 20% in Water, $\bar{M}_w \approx 340\,000$ g/mol, more than 90% hydrolyzed) was freely provided by BASF and diluted in water to obtain a 1 g/L solution. The pH of the solutions was adjusted using a 0.5 M sodium hydroxide solution. Poly(vinyl alcohol) (trade name Moviol 10-98, PVAl, $\bar{M}_w \approx 61\,000$ g/mol, 98% of hydrolysis) was purchased from Sigma-Aldrich (Lyon, France) and dissolved at 5 g/L in Milli-Q water at 80 °C and filtered over cotton wool.

Clay (EMX 2039 sodium montmorillonite) was freely provided by Clariant Produkte GmbH (Moosburg, Germany) and suspended in Milli-Q water by stirring 10 g of clay in 1 L of water for 3 days. The non-exfoliated clays were removed by centrifugation for 3 h at 5000 rpm (centrifuge 4K10 with Rotor Nr 12254 from Sigma, Lyon, France), and the supernatant was rediluted with Milli-Q water to obtain a 2.5 g/L solution (estimated from dry mass).

Sodium hydroxide pellets (>97%) were purchased from Sigma-Aldrich (Lyon, France) and diluted in Milli-Q water to obtain a 0.5 M solution. Silicon wafers (200 mm in diameter) were purchased from Wafernet Inc. (San Jose, CA) and cut in 3 × 10 cm dimensions. Octadecyltrichlorosilane (>97%) was purchased from Acros-Organics (Illkirch, France). Toluene (>99.9%) was obtained from VWR Chemical (Strasbourg, France). Ethanol absolute anhydrous (>99.9%) was obtained from Carlos Erba Reagents (Peypin, France).

Substrate Preparation. The silicon wafer (Si wafer) slides were cleaned using ethanol (10 min in ultrasound bath) and Milli-Q water (10 min in ultrasound bath) and dried using compressed air flow. Clean silicon wafers were activated for 3 min in a plasma cleaner (Harrick Plasma, Ithaca, NY) on medium intensity.

LbL Deposition. The substrate was dipped for 5 min in the PVAm solution followed by three rinsing steps of 1 min. The substrate was then dried with compressed air (typically 1 min). The same steps were applied for the deposition of CNF. This procedure consisted of one deposition cycle (layer pair) and was repeated until the desired thickness was reached.

Surface Modification of the Si Wafer. The activated silicon wafers were dipped in freshly prepared solution of octadecyltrichlorosilane 0.1% in toluene for 1 h. Then the modified substrates were cleaned with fresh toluene, ethanol, and Milli-Q water and rubbed with a dust-free cloth (Ko-ton, Chicopee Europe, AA Cuijk, The Netherlands). After surface modification, typically the thickness increased from 1.8 nm for activated silicon wafers to 4.5 nm (ellipsometry measurements).

Adhesive Layer. For silicon wafer modified with octadecyltrichlorosilane, an adhesive first layer pair was needed in order to prevent film cracking and tearing off. The clean surface modified silicon wafers were dipped in PVAl solution for 5 min followed by three rinsing steps of 1 min. After drying with compressed air, the substrate was dipped in clay solution for 5 min followed by three rinsing steps of 1 min and drying with compressed air. The substrate was then used directly for construction of the multilayer.

Automated Deposition. Preparation of the micron thick (PVAm/CNF)$_n$ multilayers was performed using a homemade dipping robot, consisting of three motorized arms (*x*,*y*,*z* directions), a drying station, an interface from ISEL (Houdan, France), and a Labview homemade program. The deposition was done according to the procedure described above in the section LbL Deposition.

Ellipsometry. For thin films (up to 3000 Å), the thickness measurements were done using a PLASMOS SD 2300 operating at a wavelength of 632.8 nm and with an angle of 70°. The refractive index was set at $n = 1.465$ and assumed to be constant. Each data point is an average of 10 measurements at random positions on the wafer. This procedure leads to slightly inexact absolute thickness values, but it allows a quick determination of the thickness and sufficient precision for the comparison of the buildup and homogeneity of the different films reported here.

For thicker films, a spectroscopic ellipsometer SENpro (SENTECH Instruments GmbH, Berlin Germany) was used. The film was modeled as a single layer with a constant refractive index of 1.55. This value was coherent with thicknesses observed by AFM and SEM and did not appear to change with the pH used during film deposition. Each thickness recorded is the average of five measurements done along the length of the sample.

Atomic Force Microscopy. Tapping mode atomic force microscopy was performed on an AFM Multimode from Bruker Nano Surface (Palaiseau, France) with the controller Nanoscope IV from Veeco (Mannheim, Germany) and noncoated silicon cantilevers (resonance frequency 300 kHz, resonance constant of 40 N/m, and radius below 10 nm). Phase and height modes were recorded simultaneously using a constant scan rate of 1.3 Hz with a resolution of 512 × 512 pixels.

In order to measure the film edges without breaking the supporting silicon wafer, a small piece of the freestanding film was cut and transferred on an activated silicon wafer. The transfer was done with the help of a drop of water on which the film is initially deposited, and after drying it with compressed air, the film laid flat on the surface.

Scanning Electron Microscopy. Films were observed with a scanning electron microscope (JEOL 6700, JEOL SAS, Croissy-sur-Seine, France) equipped with a field emission gun (SEM-FEG) at an accelerating voltage of 3 kV. The imaging was done with the SEI detector collecting secondary electrons. Before imaging, the

multilayer films were notched and carefully torn with tweezers in order to obtain a sharp edge. Samples were glued vertically with carbon tape, and about 5 nm of conductive carbon was evaporated on the surface before imaging.

UV−Visible Spectroscopy. Transmission spectra were recorded directly on the freestanding films with a Cary 5000 spectrometer from Agilent Technologies France SAS (Les Ulis, France).

X-ray Photoelectron Spectroscopy. Photoemission spectra of the film were measured on thick multilayers deposited on a silicon wafer. The measurements were performed on a Multilab 2000 (Thermo) spectrometer equipped with Al Kα anode ($h\nu$ = 1486.6 eV). The nitrogen to carbon ratio has been calculated using the sensitivity factors, as determined by Scofield[39] directly on the nitrogen and carbon peaks, respectively, at 399.7 and 285.2 eV.

Sample Preparation for Mechanical Tests. The LbL films were cut using a scalpel blade (regularly changed to prevent tearing of the film). Typically, stripes (∼1.5 mm wide and 15 mm long) were cut directly from the silicon wafer. Each stripe was then suspended with double-faced tape in a U-shaped support consisting of a 25 × 20 mm piece of paper with a 5 × 10 mm gap in the middle (Supporting Information, Figure S2a). The paper support allows easier handling and positioning of the sample in the tensile test machine.

We created a pattern on the surface of the film in order to follow the true deformation by image correlation during the tensile test (Supporting Information, Figure S2b). The pattern was made using black printer toner that electrostatically attaches to the surface of the film. The dry toner was loaded on a brush and flicked on the film from a 2 cm distance; the excess was then removed using a gentle blow of compressed air.

Mechanical Tests. A custom-made tensile test machine equipped with a 2.5 N load cell including a thermal and climatic chamber was used. The film support was fixed at the two jaws of the machine. After we cut the paper support, the film was the only bridge between the two parts of the instrument. The tensile tests were performed at constant strain rate of 0.01 mm/s at room temperature, and the force applied on the film was continuously recorded until rupture of the film occurred.

Digital Image Correlation. Because of the compliance of the machine and deformation of the tape used to fix the sample, direct measurement of the true strain of the film by the machine was impossible. Therefore, the true strain was obtained using digital image correlation.[40,41] This technique tracks the displacement of a random gray scale pattern on a sequence of images. Each image is subdivided, and a correlation algorithm is used to match the subdivisions between two images. The strain is then obtained by derivation of the displacement.

In our case, a 0.5 megapixel camera was recording the tests at 6 images/s with an image size of 1.86 × 1.40 mm. Typically, a sequence of 60 images regularly spaced were extracted from the video and imported into the digital image correlation software, CORRELISTC. Each image was subdivided into elements of 32 pixels, and reference image for the correlation algorithm was actualized every 5 images. The deformation was then averaged from 81 points (arranged on a 9 × 9 grid) and reported as true strain in the stress−strain curves. The use of relatively soft tape is compensating eventual misalignment and allows reducing partially the error on the maximal strain.

Control of Humidity. Tests run at RH ∼ 50% were performed at room conditions (actual humidity was between 45 and 55%; no modification was observed within theses values). All samples were equilibrated at room conditions for at least 24 h before measurement. Tests run at RH < 5% were carried out in a confined environment under a flow of filtered compressed air with a RH in the range of 2−3%. All samples were equilibrated before the tests for at least 24 h in a desiccator cabinet with freshly activated silica gel.

For tests done in wet conditions (RH = 100%), a drop of water was deposited on the upper surface of the film 5 min prior to testing (deposition 30 min prior to testing did not make any significant difference). In these tests, the patterning used for the measurement of the deformation was deposited on the lower surface to prevent washing off with water. These films were kept at room conditions before measurement.

Self-Repairing Experiments. A large piece (∼20 × 20 mm) is cut in a freshly prepared film. Then, the piece of film is dipped into Milli-Q water and deposited on the silicon wafer next to the rest of the initial film with a small overlap (0.6 to 2 mm). The contact was made between the two upper surfaces of the film in order to prevent interference from the adhesion layer of the film (it however did not seem to make any significant difference when the back side was put in contact with the front side). The repaired film was then gently dried with flow of compressed air. Stripes (∼1.5 mm) of films were then cut with scissors perpendicularly to the initial cut and tested with the same mechanical setup as described previously.

Conflict of Interest: The authors declare no competing financial interest.

Supporting Information Available: AFM images of $(PVAm/CNF)_8$ films built on a silicon wafer with a PVAm solution at pH = 8 and pH = 11, and optical images of a thick LbL film placed in a U-shaped support and after staining with powder toner. This material is available free of charge *via* the Internet at http://pubs.acs.org.

Acknowledgment. We gratefully acknowledge support from the Ministère de l'Enseignement Supérieur et de la Recherche, France, the Centre National de la Recherche Scientifique (CNRS), France, the International Center for Frontier Research in Chemistry, France, and the Institut Universitaire de France, France. All authors are indebted to Cedric Leuvrey (IPCMS, France) for SEM images, to Christophe Contal (ICS, France) for AFM tutorial and discussions, to Innventia AB (Sweden) for providing nanofibrillated cellulose, to BASF (Germany) for providing poly(vinyl amine) and to Lars Wågberg (KTH Royal Institute of Technology, Sweden) for fruitful discussions.

REFERENCES AND NOTES

1. Decher, G. Fuzzy Nanoassemblies: Toward Layered Polymeric Multicomposites. *Science* **1997**, *277*, 1232–1237.
2. Wang, J.; Cheng, Q.; Lin, L.; Jiang, L. Synergistic Toughening of Bioinspired Poly(vinyl alcohol)-Clay-Nanofibrillar Cellulose Artificial Nacre. *ACS Nano* **2014**, *8*, 2739–2745.
3. Wu, M.; Shuai, H.; Cheng, Q.; Jiang, L. Bioinspired Green Composite Lotus Fibers. *Angew. Chem., Int. Ed.* **2014**, *53*, 3358–3361.
4. Podsiadlo, P.; Kaushik, A. K.; Arruda, E. M.; Waas, A. M.; Shim, B. S.; Xu, J.; Nandivada, H.; Pumplin, B. G.; Lahann, J.; Ramamoorthy, A.; et al. Ultrastrong and Stiff Layered Polymer Nanocomposites. *Science* **2007**, *318*, 80–83.
5. Srivastava, S.; Kotov, N. A. Composite Layer-by-Layer (LBL) Assembly with Inorganic Nanoparticles and Nanowires. *Acc. Chem. Res.* **2008**, *41*, 1831–1841.
6. Shim, B. S.; Zhu, J.; Jan, E.; Critchley, K.; Ho, S. S.; Podsiadlo, P.; Sun, K.; Kotov, N. A. Multiparameter Structural Optimization of Single-Walled Carbon Nanotube Composites: Toward Record Strength, Stiffness, and Toughness. *ACS Nano* **2009**, *3*, 1711–1722.
7. Bieker, P.; Schönhoff, M. Linear and Exponential Growth Regimes of Multilayers of Weak Polyelectrolytes in Dependence on pH. *Macromolecules* **2010**, *43*, 5052–5059.
8. Lorencak, P.; Stange, A.; Niessner, M.; Esser, A. Polyvinylamine—A New Polymer for Increasing Paper Strength. *Wochenbl. Papierfabr.* **2000**, *128*, 14–18.
9. Gibson, L. J. The Hierarchical Structure and Mechanics of Plant Materials. *J. R. Soc. Interface* **2012**, *9*, 2749–2766.
10. Lichtenegger, H.; Reiterer, A.; Stanzl-Tschegg, S. E.; Fratzl, P. Variation of Cellulose Microfibril Angles in Softwoods and Hardwoods—A Possible Strategy of Mechanical Optimization. *J. Struct. Biol.* **1999**, *128*, 257–269.
11. Wagberg, L.; Decher, G.; Norgren, M.; Lindstroem, T.; Ankerfors, M.; Axnaes, K. The Build-up of Polyelectrolyte Multilayers of Microfibrillated Cellulose and Cationic polyelectrolytes. *Langmuir* **2008**, *24*, 784–795.
12. Wang, X.; Liu, F.; Zheng, X.; Sun, J. Water-Enabled Self-Healing of Polyelectrolyte Multilayer Coatings. *Angew. Chem., Int. Ed.* **2011**, *50*, 11378–11381.

13. Klemm, D.; Kramer, F.; Moritz, S.; Lindstrom, T.; Ankerfors, M.; Gray, D.; Dorris, A. Nanocelluloses: A New Family of Nature-Based Materials. *Angew. Chem., Int. Ed.* **2011**, *50*, 5438–5466.
14. Siro, I.; Plackett, D. Microfibrillated Cellulose and New Nanocomposite Materials: A Review. *Cellulose* **2010**, *17*, 459–494.
15. Aulin, C.; Varga, I.; Claessont, P. M.; Wagberg, L.; Lindstrom, T. Buildup of Polyelectrolyte Multilayers of Polyethyleneimine and Microfibrillated Cellulose Studied by *In Situ* Dual-Polarization Interferometry and Quartz Crystal Microbalance with Dissipation. *Langmuir* **2008**, *24*, 2509–2518.
16. Fu, J. H.; Ji, J.; Shen, L. Y.; Kueller, A.; Rosenhahn, A.; Shen, J. C.; Grunze, M. pH-Amplified Exponential Growth Multilayers: A Facile Method To Develop Hierarchical Micro- and Nanostructured Surfaces. *Langmuir* **2009**, *25*, 672–675.
17. Choi, J.; Rubner, M. F. Influence of the Degree of Ionization on Weak Polyelectrolyte Multilayer Assembly. *Macromolecules* **2005**, *38*, 116–124.
18. Feng, X.; Pelton, R.; Leduc, M.; Champ, S. Colloidal Complexes from Poly(vinyl amine) and Carboxymethyl Cellulose Mixtures. *Langmuir* **2007**, *23*, 2970–2976.
19. Geffroy, C.; Labeau, M. P.; Wong, K.; Cabane, B.; Stuart, M. A. C. Kinetics of Adsorption of Polyvinylamine onto Cellulose. *Colloids Surf., A* **2000**, *172*, 47–56.
20. Eronen, P.; Laine, J.; Ruokolainen, J.; Osterberg, M. Comparison of Multilayer Formation between Different Cellulose Nanofibrils and Cationic Polymers. *J. Colloid Interface Sci.* **2012**, *373*, 84–93.
21. Peng, C. Q.; Thio, Y. S.; Gerhardt, R. A.; Ambaye, H.; Lauter, V. pH-Promoted Exponential Layer-by-Layer Assembly of Bicomponent Polyelectrolyte/Nanoparticle Multilayers. *Chem. Mater.* **2011**, *23*, 4548–4556.
22. Yoo, D.; Shiratori, S. S.; Rubner, M. F. Controlling Bilayer Composition and Surface Wettability of Sequentially Adsorbed Multilayers of Weak Polyelectrolytes. *Macromolecules* **1998**, *31*, 4309–4318.
23. Karabulut, E.; Wagberg, L. Design and Characterization of Cellulose Nanofibril-Based Freestanding Films Prepared by Layer-by-Layer Deposition Technique. *Soft Matter* **2011**, *7*, 3467–3474.
24. Patro, T. U.; Wagner, H. D. Layer-by-Layer Assembled PVA/Laponite Multilayer Free-Standing Films and Their Mechanical and Thermal Properties. *Nanotechnology* **2011**, *22*, 455706.
25. Nogi, M.; Iwamoto, S.; Nakagaito, A. N.; Yano, H. Optically Transparent Nanofiber Paper. *Adv. Mater.* **2009**, *21*, 1595–1598.
26. Guan, Y.; Yang, S.; Zhang, Y.; Xu, J.; Han, C. C.; Kotov, N. A. Fabry-Perot Fringes and Their Application to Study the Film Growth, Chain Rearrangement, and Erosion of Hydrogen-Bonded PVPON/PAA Films. *J. Phys. Chem. B* **2006**, *110*, 13484–13490.
27. Henriksson, M.; Berglund, L. A.; Isaksson, P.; Lindstrom, T.; Nishino, T. Cellulose Nanopaper Structures of High Toughness. *Biomacromolecules* **2008**, *9*, 1579–1585.
28. Hariri, H. H.; Lehaf, A. M.; Schlenoff, J. B. Mechanical Properties of Osmotically Stressed Polyelectrolyte Complexes and Multilayers: Water as a Plasticizer. *Macromolecules* **2012**, *45*, 9364–9372.
29. Benitez, A. J.; Torres-Rendon, J.; Poutanen, M.; Walther, A. Humidity and Multiscale Structure Govern Mechanical Properties and Deformation Modes in Films of Native Cellulose Nanofibrils. *Biomacromolecules* **2013**, *14*, 4497–4506.
30. Feng, X.; Pouw, K.; Leung, V.; Pelton, R. Adhesion of Colloidal Polyelectrolyte Complexes to Wet Cellulose. *Biomacromolecules* **2007**, *8*, 2161–2166.
31. Landel, R. F.; Nielsen, L. E. *Mechanical Properties of Polymers and Composites*, 2nd ed.; Taylor & Francis: Boca Raton, FL, 1993.
32. Cranston, E. D.; Eita, M.; Johansson, E.; Netrval, J.; Salajkova, M.; Arwin, H.; Wagberg, L. Determination of Young's Modulus for Nanofibrillated Cellulose Multilayer Thin Films Using Buckling Mechanics. *Biomacromolecules* **2011**, *12*, 961–969.
33. Chung, J. Y.; Nolte, A. J.; Stafford, C. M. Surface Wrinkling: A Versatile Platform for Measuring Thin-Film Properties. *Adv. Mater.* **2011**, *23*, 349–368.
34. Bonderer, L. J.; Studart, A. R.; Gauckler, L. J. Bioinspired Design and Assembly of Platelet Reinforced Polymer Films. *Science* **2008**, *319*, 1069–1073.
35. Abe, K.; Yano, H. Cellulose Nanofiber-Based Hydrogels with High Mechanical Strength. *Cellulose* **2012**, *19*, 1907–1912.
36. Way, A. E.; Hsu, L.; Shanmuganathan, K.; Weder, C.; Rowan, S. J. pH-Responsive Cellulose Nanocrystal Gels and Nanocomposites. *ACS Macro Lett.* **2012**, *1*, 1001–1006.
37. Haraguchi, K.; Uyama, K.; Tanimoto, H. Self-Healing in Nanocomposite Hydrogels. *Macromol. Rapid Commun.* **2011**, *32*, 1253–1258.
38. Wang, Q.; Mynar, J. L.; Yoshida, M.; Lee, E.; Lee, M.; Okuro, K.; Kinbara, K.; Aida, T. High-Water-Content Mouldable Hydrogels by Mixing Clay and a Dendritic Molecular Binder. *Nature* **2010**, *463*, 339–343.
39. Scofield, J. H. Hartree-Slater Subshell Photoionization Cross-Sections at 1254 and 1487 eV. *J. Electron Spectrosc. Relat. Phenom.* **1976**, *8*, 129–137.
40. Chu, T. C.; Ranson, W. F.; Sutton, M. A.; Peters, W. H. Application of Digital-Image-Correlation Technique to Experimental Mechanics. *Exp. Mech.* **1985**, *25*, 232–244.
41. Hild, F.; Roux, S. Digital Image Correlation: From Displacement Measurement to Identification of Elastic Properties—A Review. *Strain* **2006**, *42*, 69–80.